

Optimally designed narrowband guided-mode resonance reflectance filters for mid-infrared spectroscopy

Jui-Nung Liu,^{1,2,3} Matthew V. Schulmerich,³ Rohit Bhargava,^{2,3,4,5}
and Brian T. Cunningham^{1,2,4,*}

¹Department of Electrical and Computer Engineering, University of Illinois at Urbana-Champaign, Urbana, Illinois 61801, USA

²Micro and Nanotechnology Laboratory, University of Illinois at Urbana-Champaign, Urbana, Illinois 61801, USA

³Beckman Institute for Advanced Science and Technology, University of Illinois at Urbana-Champaign, Urbana, Illinois 61801, USA

⁴Department of Bioengineering, University of Illinois at Urbana-Champaign, Urbana, Illinois 61801, USA

⁵Department of Mechanical Science and Engineering, University of Illinois at Urbana-Champaign, Urbana, Illinois 61801, USA

*bcunning@illinois.edu

Abstract: An alternative to the well-established Fourier transform infrared (FT-IR) spectrometry, termed discrete frequency infrared (DFIR) spectrometry, has recently been proposed. This approach uses narrowband mid-infrared reflectance filters based on guided-mode resonance (GMR) in waveguide gratings, but filters designed and fabricated have not attained the spectral selectivity ($\leq 32 \text{ cm}^{-1}$) commonly employed for measurements of condensed matter using FT-IR spectroscopy. With the incorporation of dispersion and optical absorption of materials, we present here optimal design of double-layer surface-relief silicon nitride-based GMR filters in the mid-IR for various narrow bandwidths below 32 cm^{-1} . Both shift of the filter resonance wavelengths arising from the dispersion effect and reduction of peak reflection efficiency and electric field enhancement due to the absorption effect show that the optical characteristics of materials must be taken into consideration rigorously for accurate design of narrowband GMR filters. By incorporating considerations for background reflections, the optimally designed GMR filters can have bandwidth narrower than the designed filter by the antireflection equivalence method based on the same index modulation magnitude, without sacrificing low sideband reflections near resonance. The reported work will enable use of GMR filters-based instrumentation for common measurements of condensed matter, including tissues and polymer samples.

©2011 Optical Society of America

OCIS codes: (050.0050) Diffraction and gratings; (050.1970) Diffraction optics; (310.0310) Thin films; (310.2790) Guided waves; (300.6340) Spectroscopy, infrared; (300.6300) Spectroscopy, Fourier transforms.

References and links

1. L. Mashev and E. Popov, "Zero order anomaly of dielectric coated gratings," *Opt. Commun.* **55**(6), 377–380 (1985).
2. H. Bertoni, L. Cheo, and T. Tamir, "Frequency-selective reflection and transmission by a periodic dielectric layer," *IEEE Trans. Antenn. Propag.* **37**(1), 78–83 (1989).
3. M. T. Gale, K. Knop, and R. H. Morf, *Proc. Soc. Photo Opt. Instrum. Eng.* **1210**, 83 (1990).
4. B. T. Cunningham, P. Li, B. Lin, and J. Pepper, "Colorimetric resonant reflection as a direct biochemical assay technique," *Sens. Actuators B Chem.* **81**(2-3), 316–328 (2002).
5. B. T. Cunningham, B. Lin, J. Qiu, P. Li, J. Pepper, and B. Hugh, "A plastic colorimetric resonant optical biosensor for multiparallel detection of label-free biochemical interactions," *Sens. Actuators B Chem.* **85**(3), 219–226 (2002).

6. L. L. Chan, M. F. Pineda, J. T. Heeres, P. J. Hergenrother, and B. T. Cunningham, "A General Method for Discovering Inhibitors of Protein-DNA Interactions using Photonic Crystal Biosensors," *ACS Chem. Biol.* **3**(7), 437–448 (2008).
7. P. C. Mathias, N. Ganesh, W. Zhang, and B. T. Cunningham, "Graded Wavelength One-Dimensional Photonic Crystal Reveals Spectral Characteristics of Enhanced Fluorescence," *J. Appl. Phys.* **103**(9), 094320 (2008).
8. P. C. Mathias, H.-Y. Wu, and B. T. Cunningham, "Employing two distinct photonic crystal resonances for improved fluorescence enhancement," *Appl. Phys. Lett.* **95**(2), 021111 (2009).
9. A. Pokhriyal, M. Lu, V. Chaudhery, C.-S. Huang, S. Schulz, and B. T. Cunningham, "Photonic crystal enhanced fluorescence using a quartz substrate to reduce limits of detection," *Opt. Express* **18**(24), 24793–24808 (2010).
10. F. Yang, G. Yen, and B. T. Cunningham, "Integrated 2D photonic crystal stack filter fabricated using nanoreplica molding," *Opt. Express* **18**(11), 11846–11858 (2010).
11. G. Niederer, H. P. Herzig, J. Shamir, H. Thiele, M. Schnieper, and C. Zschokke, "Tunable, Oblique Incidence Resonant Grating Filter for Telecommunications," *Appl. Opt.* **43**(8), 1683–1694 (2004).
12. S. T. Thurman and G. M. Morris, "Controlling the Spectral Response in Guided-Mode Resonance Filter Design," *Appl. Opt.* **42**(16), 3225–3233 (2003).
13. M. G. Moharam, E. B. Grann, D. A. Pomet, and T. K. Gaylord, "Formulation for stable and efficient implementation of the rigorous coupled-wave analysis of binary gratings," *J. Opt. Soc. Am. A* **12**(5), 1068–1076 (1995).
14. M. G. Moharam, D. A. Pomet, E. B. Grann, and T. K. Gaylord, "Stable implementation of the rigorous coupled-wave analysis for surface-relief gratings: enhanced transmittance matrix approach," *J. Opt. Soc. Am. A* **12**(5), 1077–1086 (1995).
15. D. Shin, S. Tibuleac, T. A. Maldonado, and R. Magnusson, "Thin-film optical filters with diffractive elements and waveguides," *Opt. Eng.* **37**(9), 2634–2646 (1998).
16. Z. Hegedus and R. Netterfield, "Low Sideband Guided-Mode Resonant Filter," *Appl. Opt.* **39**(10), 1469–1473 (2000).
17. S. Tibuleac and R. Magnusson, "Narrow-linewidth bandpass filters with diffractive thin-film layers," *Opt. Lett.* **26**(9), 584–586 (2001).
18. G. Bao and K. Huang, "Optimal design of guided-mode grating resonance filters," *IEEE Photon. Technol. Lett.* **16**(1), 141–143 (2004).
19. G. Bao and K. Huang, "Computational design for guided-mode grating resonances," *J. Opt. Soc. Am. A* **22**(7), 1408–1413 (2005).
20. W. Liu, Z. Lai, H. Guo, and Y. Liu, "Guided-mode resonance filters with shallow grating," *Opt. Lett.* **35**(6), 865–867 (2010).
21. D. C. Fernandez, R. Bhargava, S. M. Hewitt, and I. W. Levin, "Infrared spectroscopic imaging for histopathologic recognition," *Nat. Biotechnol.* **23**(4), 469–474 (2005).
22. R. Bhargava, "Towards a practical Fourier transform infrared chemical imaging protocol for cancer histopathology," *Anal. Bioanal. Chem.* **389**(4), 1155–1169 (2007).
23. A. K. Kodali, M. Schulmerich, J. Ip, G. Yen, B. T. Cunningham, and R. Bhargava, "Narrowband midinfrared reflectance filters using guided mode resonance," *Anal. Chem.* **82**(13), 5697–5706 (2010).
24. R. Bhargava, D. C. Fernandez, S. M. Hewitt, and I. W. Levin, "High throughput assessment of cells and tissues: Bayesian classification of spectral metrics from infrared vibrational spectroscopic imaging data," *Biochim. Biophys. Acta* **1758**(7), 830–845 (2006).
25. S. S. Wang and R. Magnusson, "Theory and applications of guided-mode resonance filters," *Appl. Opt.* **32**(14), 2606–2613 (1993).
26. S. S. Wang and R. Magnusson, "Design of waveguide-grating filters with symmetrical line shapes and low sidebands," *Opt. Lett.* **19**(12), 919–921 (1994).
27. A. Sharon, D. Rosenblatt, and A. A. Friesem, "Resonant grating-waveguide structures for visible and near-infrared radiation," *J. Opt. Soc. Am. A* **14**(11), 2985–2993 (1997).
28. D. Rosenblatt, A. Sharon, and A. A. Friesem, "Resonant grating waveguide structures," *IEEE J. Quantum Electron.* **33**(11), 2038–2059 (1997).
29. S. L. Chuang, *Physics of Optoelectronic Devices* (Wiley, New York, 1995).
30. A. Yariv and P. Yeh, *Photonics: Optical Electronics in Modern Communications*, 6th ed. (Oxford U. Press, New York, 2007).
31. M. Klanjšek Gunde and M. Maček, "Infrared Optical Constants and Dielectric Response Functions of Silicon Nitride and Oxynitride Films," *Phys. Status Solidi* **183**, 439–449 (2001).
32. M. Rubin, "Optical properties of soda lime silica glasses," *Sol. Energy Mater.* **12**(4), 275–288 (1985).
33. S. M. Norton, G. M. Morris, and T. Erdogan, "Experimental investigation of resonant-grating filter lineshapes in comparison with theoretical models," *J. Opt. Soc. Am. A* **15**(2), 464–472 (1998).
34. T. Sun, J. Wang, J. Ma, Y. Jin, H. He, J. Shao, and Z. Fan, "Ultra-narrow bandwidth resonant reflection grating filters using the second diffracted orders," *Opt. Commun.* **282**(4), 451–454 (2009).
35. T. Sun, J. Ma, J. Wang, Y. Jin, H. He, J. Shao, and Z. Fan, "Electric field distribution in resonant reflection filters under normal incidence," *J. Opt. A, Pure Appl. Opt.* **10**(12), 125003 (2008).
36. J. N. Liu, M. Schulmerich, R. Bhargava, and B. T. Cunningham, University of Illinois at Urbana-Champaign, Urbana, IL are preparing a manuscript to be called "Effects of collimation on narrowband guided-mode resonance filters in mid-infrared,"

37. S. S. Wang and R. Magnusson, "Multilayer waveguide-grating filters," *Appl. Opt.* **34**(14), 2414–2420 (1995).
38. A. L. Fehrembach, A. Talneau, O. Boyko, F. Lemarchand, and A. Sentenac, "Experimental demonstration of a narrowband, angular tolerant, polarization independent, doubly periodic resonant grating filter," *Opt. Lett.* **32**(15), 2269–2271 (2007).
-

1. Introduction

Since the introduction of narrowband reflectance filters using subwavelength periodic grating nanostructures [1–3], guided-mode resonance (GMR) filters (as they have come to be called, but also known as photonic crystal slabs or photonic crystal surfaces) have found application in label-free biodetection [4–6], fluorescence enhancement [7–9], optical limiting [10], and telecommunications [11, 12]. Despite the large number of papers that utilize electromagnetic simulation methods such as rigorous coupled wave analysis (RCWA) [13, 14] to study and design GMR filters, none fully consider the effects of optical losses from the materials that the GMR filter is comprised of and the resulting effects of optical loss upon the resonant filter characteristics. Indeed, for filter design that must meet stringent performance criteria that include filter bandwidth, out-of-band rejection, and filter efficiency, these considerations become critical for determining whether or not a design is feasible with a set of materials. Without the effects of optical loss, GMR filters may be designed to provide ~100% reflection efficiency and vanishingly small bandwidth [15–20], but real materials often fail to be completely lossless. Optical properties of GMR filters such as the resonance wavelength, peak reflection efficiency, and resonant linewidth are heavily dependent upon the complex refractive index of materials which is a function of wavelength, so it is actually necessary to consider the dispersion ($dn/d\lambda \neq 0$ and $d\kappa/d\lambda \neq 0$, where n and κ are the real and imaginary part of the complex refractive index, respectively) of optical materials to obtain designs that accurately reflect experimentally measured behavior. With accurate incorporation of material parameters into design models, it is possible to adjust the dimensional parameters of a GMR filter to achieve a particular resonant wavelength. For practical fabrication of devices, it is desirable to adjust dimensional parameters that are easily controlled (such as grating height and thin film layer thickness) in contrast to parameters that are adjustable only with increased cost or effort (such as grating fill factor).

An application for which accurate GMR filters design is especially critical is infrared (IR) absorption spectroscopic imaging. The efficiency and expense of IR imaging spectroscopy can be greatly improved using narrowband filters for applications such as automated cancer pathology [21, 22] by acquisition of data only from a few specific regions in the spectrum that correspond to known spectral features that differentiate cell and disease types [23, 24]. Compared to Fourier Transform Infrared (FTIR) spectroscopic imaging, discrete-frequency IR (DFIR) spectroscopy can be performed rapidly with simple and inexpensive instrumentation due to elimination of the need for an interferometer for spectral selectivity. DFIR spectroscopy requires a set of optical filters with narrow bandwidth (typically $\leq 32 \text{ cm}^{-1}$ for solids and liquids) for spectroscopy. One method for obtaining illumination from these wavelengths is to reflect a broadband light source against a resonant reflectance filter, such as a GMR filter and to direct the narrow band of reflected wavelengths through a biological sample. In DFIR spectroscopy, a set of GMR filters with predetermined resonant wavelengths are illuminated by the broadband light source in sequence, and separate absorption intensity images are gathered for each wavelength using an appropriate infrared imaging camera, such as a microbolometer array. For DFIR spectroscopy to be effective, it is necessary to fabricate a series of GMR filters that simultaneously provide high reflectance efficiency for the resonant wavelength, low out-of-band reflectance, and narrow bandwidth. In our recent work, GMR filters in the mid-IR were demonstrated [23]. RCWA simulations incorporating the absorption and dispersion of materials were used to design GMR filter structures, where bandwidth of the designed filters is larger than 32 cm^{-1} and background reflection reaches up to 17% near resonance wavenumbers. Spectroscopic measurements of a set of fabricated

filters were compared with theory with good agreement. In order to realize GMR filters with bandwidth $\leq 32 \text{ cm}^{-1}$ and lower sideband reflections for DFIR spectroscopy, design optimization of filter structures is essential to guide for fabrication.

In this paper, we describe a design optimization approach for obtaining narrow bandwidth GMR filters in the mid-IR, with absorption and dispersion characteristics of materials taken into consideration. We first study the impact of absorption and dispersion of materials on GMR filters when bandwidth becomes narrow. Second, we describe how to achieve an optimal GMR filter design at one specific resonance wavenumber for various bandwidths. Finally, we compare the optimal filter design developed in this paper and the filter design with conventional antireflection (AR) equivalence method. Although we focus upon design of GMR filters in the mid-IR part of the spectrum, the approach described in this work can be extended to any wavelength.

2. GMR structure and physical principle

The double-layer GMR filter in this study has a Si_3N_4 surface-relief periodic grating structure built on top of a soda lime glass substrate. The grating period (Λ), grating depth (d^{gr}), and waveguide layer thickness (d^{wg}) of the GMR filter structure are depicted in Fig. 1. Thin film layer of Si_3N_4 can be easily deposited onto the substrate by plasma enhanced chemical vapor deposition (PECVD), and can be etched using reactive ion etching (RIE). In addition to simple fabrication, Si_3N_4 has a transparent window in mid-IR ($\lambda < \sim 6 \mu\text{m}$), making it an appropriate material candidate for GMR filters in a DFIR instrument that can be used to measure absorption caused by C-H, O-H and S-H stretching vibrational modes ($> 2600 \text{ cm}^{-1}$).

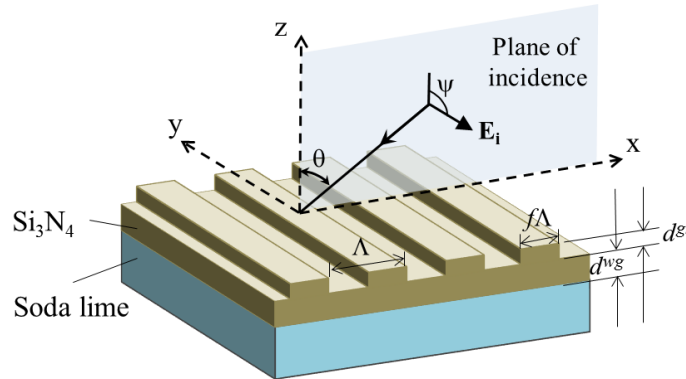


Fig. 1. GMR filter design comprised on a soda lime glass substrate, a Si_3N_4 waveguide/grating layer, and an air superstrate. The device is illuminated from the superstrate side at normal incidence with a plane wave polarized parallel to the grating lines for excitation of TE modes, and with a plane wave polarized perpendicular to the grating lines for TM modes.

The optical phenomenon behind the narrowband reflectance properties of GMR filters has been described previously [25–28] but is briefly summarized here. When a plane electromagnetic wave is incident on the GMR filter at a wavelength for which there is no guided-mode resonance, the transmission and reflection spectra can be understood using conventional thin-film theory [26]. However, a guided wave can be excited if the incident light meets the Bragg diffraction condition [29, 30]:

$$k_0 n_c \sin \theta \pm p \left(\frac{2\pi}{\Lambda} \right) = \beta \quad (1)$$

where k_0 is the wave vector in free space, n_c is the index of the refractive index in the cover region (free space), p is the diffraction order and is an integer, and β is the propagation wave vector in the GMR layer structure. The guided propagating wave experiences scattering into

specular and transmitted directions assisted by the grating periodic structure as well as optical absorption in the waveguide layer structure. For this reason, such guided modes are also called “leaky modes.” The constructive interference of waves in the specular direction creates peak reflection efficiency; at the same time the destructive interference of waves in the transmitted direction generates a dip in the transmission spectra [27, 28]. The filter property of GMR filters can be used to admit light in a small region of the spectrum, with light outside the reflection band being rejected. When illuminated at the resonant condition, the guided mode in GMR filters is not only excited and extracted simultaneously via periodic grating structures, but is also coupled to the guided wave propagating along the other direction via Bragg diffraction. The constructive interference of the two counter-propagating guided waves establishes an electromagnetic standing wave, leading to near-field enhancement and storage of photon energy.

3. Results and discussion

3.1 Effects of dispersion and absorption of optical materials on narrowband GMR filters

With ideal, lossless materials, the bandwidth of a GMR filter can be reduced by simply decreasing the grating depth d^{gr} [20]. As the grating depth decreases, the coupling loss of the leaky modes becomes weaker, resulting in a longer photon lifetime in the GMR structures and hence a narrower resonance linewidth. To illustrate this effect, we simulated the reflectance spectra of three filters with different layer thicknesses using RCWA, as shown in Fig. 2 (a). The three structures of $d^{gr} = 300, 150,$ and 50 nm have a peak reflectance $\sim 100\%$ at resonance wavenumbers of $2659, 2588,$ and 2549 cm^{-1} , respectively, with distinct FWHM bandwidth of $31, 8,$ and 1 cm^{-1} , respectively. Conservation of power requires $R + T + A = 1$, where $R, T,$ and A are reflectance, transmittance, and absorbance, respectively. Because $R \sim 100\%$ at the resonant wavenumber and $A = 0$, the transmittance at the resonant wavenumber is close to zero for filters without material absorption.

When there is material absorption in the GMR structure, the transmittance at the resonant wavenumber will become greater than zero based on the multiple interference model of GMR structures [27, 28], leading to peak reflectance lower than 100% . In Fig. 2(b), we show the effect on resonances of the dispersion and absorption properties of both Si_3N_4 [31] and soda lime glass [32] for three filters with different layer thicknesses. Due to variation of refractive index, the resonances occur at different wavenumbers of $2662, 2597,$ and 2559 cm^{-1} for filters with $d^{gr} = 300, 150,$ and 50 nm, respectively, indicating that the dispersion effect must be considered for accurate design of narrowband GMR filters. Although the exact resonance wavenumbers of GMR filters have to be determined numerically by using RCWA method, it is meaningful to get more physical insight by studying red shift of the resonance wavenumbers with dispersion curves for a simplified dielectric waveguide when the grating depth is small enough, as shown in Fig. 2(c). The guided modes locate between two light lines for Si_3N_4 and soda lime because of waveguide guidance conditions. For normal incidence the phase matching condition requires the propagation wavevector $\beta = (2\pi)/\Lambda$. The intercept point between TE_0 dispersion curve and the straight line $\beta = (2\pi)/\Lambda$ gives the spectral location of the TE_0 guided-mode resonance. When dispersion of material is considered, the refractive indices of Si_3N_4 and soda lime near 2550 cm^{-1} (close to the resonance wavenumber of the filter with $d^{gr} = 50$ nm) will be slightly smaller than the constant refractive indices used in Fig. 2(a), which decreases the slopes of the light lines and shifts the dispersion curves toward higher wavenumbers. The effect is further illustrated in Fig. 2(d), indicating a red shift of ~ 10 cm^{-1} when dispersion of materials is considered. Decreasing the grating depth of GMR filters with material absorption cannot only narrow filter bandwidth, but also reduce peak reflectance as shown in Fig. 2(b), in contrast to the previous case without considering dispersion and absorption of materials as shown in Fig. 2(a). When the grating depth is smaller, the ratio of coupling loss to dissipation loss becomes smaller, resulting in reduction of the peak reflection

efficiency [12, 27, 28, 33]. Therefore, for GMR filters with material absorption, the inherent tradeoff between bandwidth and reflection efficiency puts a limitation on performance of narrowband GMR filters, and the design method of narrowband filters needs to be improvised as simply decreasing the grating layer thickness to obtain GMR filters with narrow linewidth [20] is not effective.

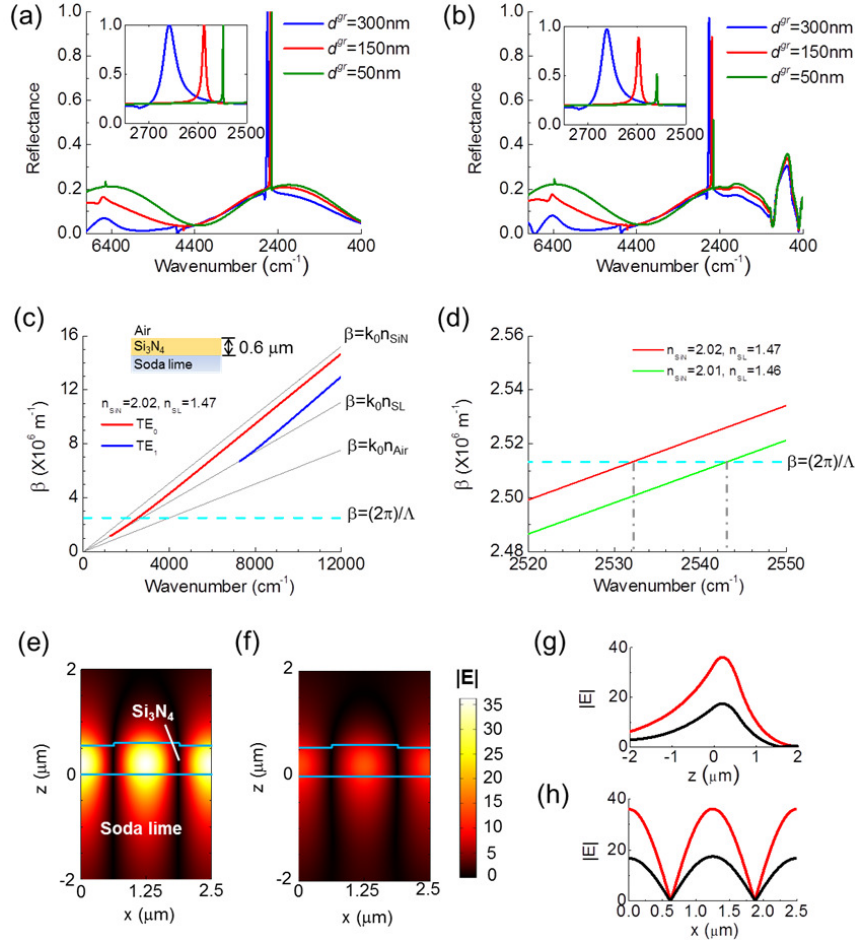


Fig. 2. Effect on guided-mode resonances of dispersion and absorption properties of Si_3N_4 and soda lime, when a TE-polarized wave is normally incident on GMR filters with grating period $\Lambda = 2.5\text{ }\mu\text{m}$, duty cycle $f = 0.5$, and Si_3N_4 total thickness $d^{\text{gr}} + d^{\text{ng}} = 0.6\text{ }\mu\text{m}$. (a) Reflectance spectra of three filters with different grating depths without considering the dispersion characteristics of both Si_3N_4 and soda lime. The refractive indices chosen are $n_{\text{SiN}} = 2.02$ and $n_{\text{SL}} = 1.47$. (b) Reflectance spectra considering the dispersion characteristics of both Si_3N_4 [31] and soda lime glass [32]. (c) The dispersion relation for a simplified dielectric waveguide, where the refractive indices used are the same as those in (a). The phase matching condition requires $\beta = (2\pi)/\Lambda$, where the grating period $\Lambda = 2.5\text{ }\mu\text{m}$. (d) Explanation of the observed red shift of guided mode resonances by comparing dispersion curves for the TE_0 mode using $n_{\text{SiN}} = 2.01$ and $n_{\text{SL}} = 1.46$ near 2550 cm^{-1} with that in (c). (e-f) Distribution of the electric field amplitude ($|E|$) in a unit cell of the filter with grating depth $d^{\text{gr}} = 50\text{ nm}$ for illumination at (e) $\nu = 2549\text{ cm}^{-1}$ without considering the dispersion characteristics of both Si_3N_4 and soda lime and at (f) $\nu = 2559\text{ cm}^{-1}$ considering the dispersion properties of both Si_3N_4 and soda lime. (g-h) Comparison of electric field amplitude profiles shown in (e) and (f) at $x = 1.25\text{ }\mu\text{m}$ (left) and near the center of the waveguide layer at $z = 200\text{ nm}$ (right).

The material absorption influences not only the spectral response of GMR filters but also their electric field enhancement. In Fig. 2(c) we show the electric field enhancement

distribution in a GMR structure ($d^{gr} = 50$ nm) at a resonant wavenumber (2549 cm^{-1}) without considering material absorption, which is lower at a resonance wavenumber (2559 cm^{-1}) when material absorption is considered, as shown in Fig. 2(d). The standing wave patterns in both cases build up because two counter-propagating waves (diffraction order $p = \pm 1$) are coupled together via distributed feedback provided by periodic grating structures. Presence of material absorption in GMR filters decreases the propagation length of the two counter-propagating coupled waves and then lowers the number of photons participating in the multiple interference, resulting in a smaller on-resonance electric field enhancement. Comparison of E-field enhancement profiles are plotted in Fig. 2(e) and (f) in order to further illustrate the effect of material absorption on resonances of narrowband GMR filters. The ratio of maximum E-field enhancement in the GMR structure of $d^{gr} = 50$ nm without considering dispersion and absorption of materials to the maximum enhancement when dispersion and absorption of materials are considered is 2.07, whereas the ratio is only slightly larger than 1 for GMR filter with $d^{gr} = 300$ nm and larger bandwidth [23], which implies that optical absorption of materials significantly impacts narrowband GMR filters much more than GMR filters with wide bandwidth. In summary, we note that absorption and dispersion characteristics of optical materials can impact performance of GMR filters when the filter bandwidth becomes narrow.

3.2 Considerations for higher-order modes

Higher-order TE_m or TM_m ($m = 1, 2, 3, \dots$) guided mode resonance has been investigated [34] and may appear when the waveguide layer thickness is large enough. For DFIR imaging spectroscopy of biopsy specimens, the spectral region of interest ranges from $\sim 950 \text{ cm}^{-1}$ (cutoff of the mid-IR array detector) to $\sim 4000 \text{ cm}^{-1}$ (upper limit of useful spectral information). The filters for optical spectroscopy thus are not only required to have bandwidth narrow enough to acquire IR absorption information contained in small spectral regions, but it is also necessary to have only a single reflection peak over the entire spectral range of interest, which means that higher-order modes in GMR filters must be cut off.

If the grating depth is small enough, the optical modes in GMR filters can be understood using the theory of dielectric slab waveguides by assuming $d^{gr} = 0$ for simplicity as an approximation [29]. Higher-order waveguide modes occur when the waveguide layer thickness is large, so the waveguide layer of GMR filters must be thin enough to suppress the propagation of higher-order modes. At cutoff the decay constant along the z direction in the substrate region vanishes, and therefore the propagation wavevector $\beta = k_0 n_{SL}$. We can then estimate the cutoff thickness for the TE_1 and TM_1 waveguide modes based on their cutoff conditions [29, 30]:

$$k_0 d \sqrt{n_{SiN}^2 - n_{SL}^2} = \tan^{-1} \frac{\sqrt{n_{SL}^2 - n_{Air}^2}}{\sqrt{n_{SiN}^2 - n_{SL}^2}} + \pi \quad (\text{TE}_1) \quad (2)$$

$$k_0 d \sqrt{n_{SiN}^2 - n_{SL}^2} = \tan^{-1} \frac{n_{SiN}^2 \sqrt{n_{SL}^2 - n_{Air}^2}}{n_{Air}^2 \sqrt{n_{SiN}^2 - n_{SL}^2}} + \pi \quad (\text{TM}_1) \quad (3)$$

By assuming $n_{SiN} = 2$ and $n_{SL} = 1.48$, we calculate a cutoff waveguide thickness $d^{wg} = 1.13 \text{ }\mu\text{m}$ for the TE_1 mode and $d^{wg} = 1.31 \text{ }\mu\text{m}$ for the TM_1 mode at 4000 cm^{-1} . However, for GMR filters with peak reflectance high enough to be useful, the ratio of coupling loss to dissipation loss needs to be large enough [12, 27, 28, 33], so the grating depth must not be too small. Consequently, an approximation method that neglects the grating layer cannot accurately predict cutoff conditions of higher-order modes, although the approximation can give a rough estimate of the cutoff thickness.

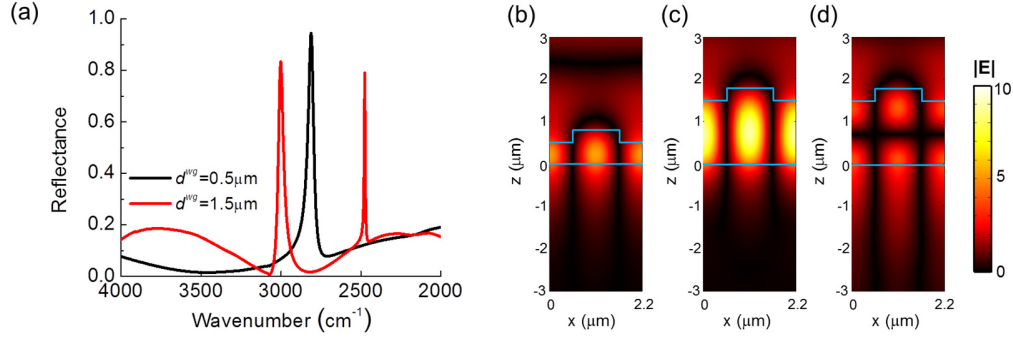


Fig. 3. Effect on reflectance spectra of higher-order modes. Reflectance spectra of two filters when a TE-polarized wave is normally incident. Grating period $\Lambda = 2.2$ mm, grating depth $d^{gr} = 0.3$ μm , waveguide layer thickness $d^{wg} = 0.5$ μm (black), and $d^{wg} = 1.5$ μm (red). (b-d) Electric field amplitude distribution of (b) the TE_0 mode at a resonance wavenumber ($\nu = 2811$ cm^{-1}) for structure of $d^{wg} = 0.5$ μm , (c) the TE_0 mode at a resonance wavenumber ($\nu = 2475$ cm^{-1}) and (d) the TE_1 mode at a resonance wavenumber ($\nu = 3001$ cm^{-1}) for structure of $d^{wg} = 1.5$ μm .

Using RCWA, we simulated the spectral response of GMR filters with different waveguide layer thicknesses when TE-polarized light is normally incident, as shown in Fig. 3(a). The filter with $d^{wg} = 0.5$ μm has only one reflection peak at 2811 cm^{-1} , corresponding to resonance of the TE_0 mode as shown in Fig. 3(b). For the GMR structure of $d^{wg} = 1.5$ μm the reflection peak at 2475 cm^{-1} corresponds to the resonance of the TE_0 mode and has a narrower linewidth compared to the resonance of the TE_0 mode in the structure with $d^{wg} = 0.5$ μm , leading to a higher E -field enhancement as shown in Fig. 3(c) [35]. In addition to resonance of the TE_0 mode, the GMR filter with greater waveguide layer thickness has an additional reflection peak at 3001 cm^{-1} , corresponding to resonance of the TE_1 mode as shown in Fig. 3(d). The field distribution profile shows that the decay constant along the z -direction of the TE_1 mode in the substrate region is smaller than that of the TE_0 mode, indicating that the TE_1 mode is near cutoff. Because cutoff thickness depends on both layer thicknesses and the grating period, it is necessary to pay attention to the occurrence of higher-order modes over the spectral region of interest while varying these geometric parameters.

3.3 Design GMR filters for spectroscopy

In this section, we perform design optimization of GMR filters with a resonance wavenumber of 2600 cm^{-1} , because there is a local minimum for absorption of Si_3N_4 near this wavenumber [31]. The optimal design approach can apply to any other wavenumber where material absorption and dispersion are present. The resonance wavenumber, peak reflectance, and filter bandwidth of GMR filters all are dependent on the structure parameters such as grating depth d^{gr} , waveguide layer thicknesses d^{wg} , grating period Λ , and grating filling factor f . Conventionally, in order to reduce sideband reflections the layer thicknesses of GMR filters are required to meet the antireflection (AR) condition, and grating period is then finely adjusted in order to match the resonance wavenumber of GMR filters with the targeted resonance wavenumber [15, 20]. The grating filling factor f is another parameter that may also be changed to match the targeted resonance wavenumber [18, 19]. However, the structure parameters which can be finely tuned using planar photolithography, thin-film deposition, and etching processes are layer thicknesses rather than the grating period and filling factor.

The design optimization procedure developed in this work is illustrated in Fig. 4. Instead of continuously changing filling factor and grating period, we fix the grating filling factor $f = 0.5$, as this value is simplest to obtain experimentally [23], and we choose several discrete period values based on the inequality for resonance regime of GMR filters [25]:

$$\max\{n_c, n_s\} \leq \left| n_c \sin \theta - \frac{p}{\nu \Lambda} \right| \leq \max\{n_{gr}, n_{wg}\} \quad (4)$$

where p is the order of diffracted waves propagating in the waveguide layer, and n_s , n_{gr} , and n_{wg} are the refractive indices of the substrate, the grating, and the waveguide layer, respectively. Here the refractive indices are assumed to be $n_c = 1$, $n_{gr} = n_{wg} = n_{SiN} = 2.01$ and $n_s = n_{SL} = 1.47$ at $\nu = 2600 \text{ cm}^{-1}$, and the incident angle $\theta = 0$ at normal incidence for easier experimental setup. Accordingly, the grating period approximately obeys $1.91 < \Lambda < 2.62 \text{ }\mu\text{m}$, and we choose discrete periods $\Lambda = 2.0, 2.1, 2.2, 2.3, 2.4, 2.5$, and $2.6 \text{ }\mu\text{m}$.

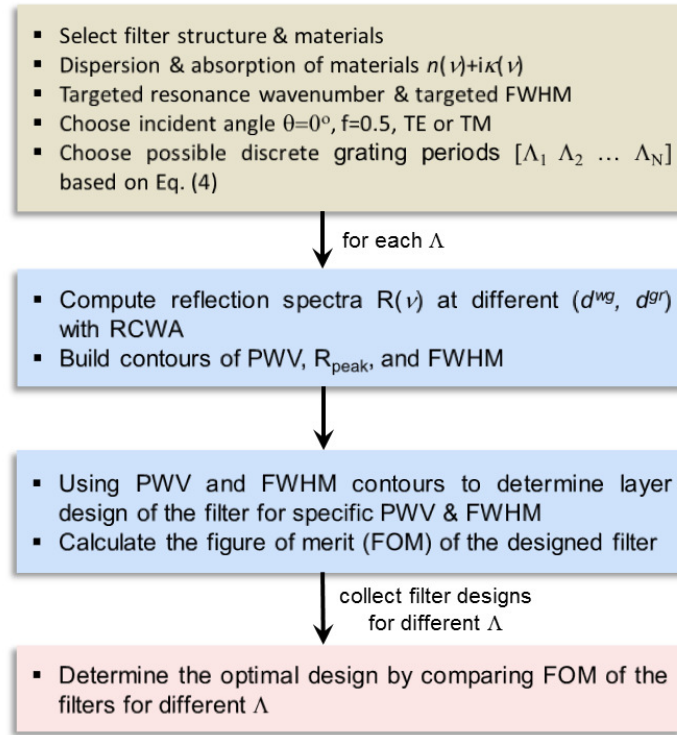


Fig. 4. Schematic of the design optimization procedure for reflection narrowband GMR filters.

Because the refractive index in the cover region n_c and refractive index in the substrate region n_{SL} are different, the band shape of the GMR filters can be asymmetric [26]. Therefore, we extract peak wavenumber values (PWVs) and FWHM bandwidth of GMR filters by fitting the spectral response with a Lorentzian:

$$R(\nu) = R_0 + (R_{peak} - R_0) \frac{\Delta \nu}{2/\pi} \frac{\Delta \nu / (2\pi)}{(\nu - \nu_0)^2 + (\Delta \nu / 2)^2} \quad (5)$$

where R_0 is the background reflectance near resonance, R_{peak} is the peak reflectance calculated by RCWA, $\Delta \nu$ is the FWHM bandwidth, and ν_0 is the PWV. In this equation, R_0 , $\Delta \nu$, and ν_0 are fitted by minimizing the standard error of the fit, as shown in Fig. 5(a). By integrating $I(\nu)R(\nu)$ over all ν in the spectral region above cutoff of the detector, we can estimate the reflected power received by the detector in IR spectroscopy. In DFIR, both the signal within the reflection band and any out-of-band photons contributed by the background or sideband reflections contribute to the detected intensity. Therefore, the ratio of the in-band integration I_{IB} to the out-of-band integration I_{OB} , as shown in Fig. 5(b), depicts the quality of filters for

acquisition of data in a small portion of the spectrum. The ratio I_{IB}/I_{OB} must therefore be large; otherwise the signal within the reflection band will be overwhelmed by the sideband reflection signal. Besides, the value of the out-of-band integration I_{OB} depends on the boundaries of integration or spectral regions, and the sideband signal can be effectively reduced if an IR bandpass filter is used in series with a narrowband GMR filter. The characteristics of GMR filters comprising PWV, R_{peak} , FWHM bandwidth, and I_{IB}/I_{OB} will be used to evaluate performance of the designed filters for various narrow bandwidths.

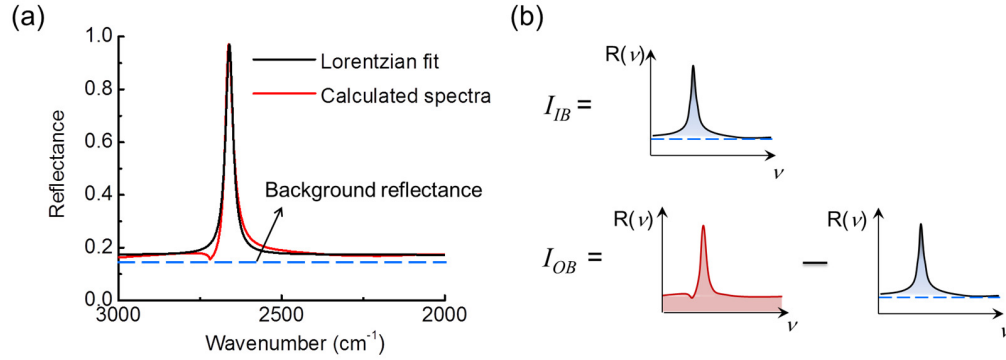


Fig. 5. (a) Calculated reflectance spectra of a GMR filter with $\Lambda = 2.5 \mu\text{m}$, $d^{wg} = 0.3 \mu\text{m}$, and $d^{gr} = 0.3 \mu\text{m}$. The peak wavenumber value (PWV) and the filter bandwidth (full width at half-maximum, or FWHM) are determined by Lorentzian curve fitting. (b) Illustration of the in-band integration (I_{IB}) and the out-of-band integration (I_{OB}).

We calculate PWV, FWHM bandwidth, and R_{peak} of GMR filters as a function of d^{gr} , d^{wg} , and chosen grating periods Λ for normally incident TE-polarized and TM-polarized illumination in order to get contour maps of filter properties, as shown in Fig. 6 and Fig. 7. The blank areas in the contour plots correspond to the layer thicknesses having $R_{peak} < 0.3$, which is too small to be useful for IR spectroscopy. The optical properties of GMR filters have close relationship to the geometric parameters. For each grating period Λ , the propagation constant β of two counter-propagating waves has to meet the Bragg diffraction condition $\Delta\beta = 2\beta = G$, where $G = m(2\pi/\Lambda)$ is the reciprocal lattice vector of the 1-D periodic grating structure and m is an integer [29, 30]. The thicker the waveguide layer, the smaller the wave vector along the z -direction (k_z) in the waveguide layer. Because of the dispersion relation $k_0^2 n_{\text{SiN}}^2 = \omega^2 (\mu_0 \epsilon_{\text{SiN}})^{1/2} = k_z^2 + \beta^2$, smaller k_z leads to a smaller PWV. In addition, decreasing d^{gr} reduces the coupling loss of the leaky modes and FWHM bandwidth, resulting in smaller R_{peak} due to material absorption. When both d^{gr} and d^{wg} are small enough, the TE_0 mode cannot be guided, based on the theory of asymmetric dielectric slab waveguides [29], leading to the bottom-left blank area in each contour plot. Resonances of the TE_1 mode occur when d^{wg} is near $1.2 \mu\text{m}$, which therefore defines the right boundary of the contour plots for filter design. As the grating period Λ increases from 2.2 to $2.6 \mu\text{m}$, the on-resonance propagation constant β decreases (Bragg condition), and therefore the overall PWV distribution shifts toward lower wavenumbers based on the dispersion relation. Because Si_3N_4 has a local minimum absorption near $2500\text{--}2600 \text{ cm}^{-1}$, filters with larger grating period have narrower bandwidth and larger R_{peak} . In addition to TE-polarization, we also study the TM case as shown in Fig. 7. The resonance locations for TE and TM polarizations are different, and the average bandwidth for TM is smaller. When increasing d^{wg} until near $1.4 \mu\text{m}$, resonances of the TM_1 mode begin to occur, making the boundaries of the contour plots different for TE and TM-polarization cases.

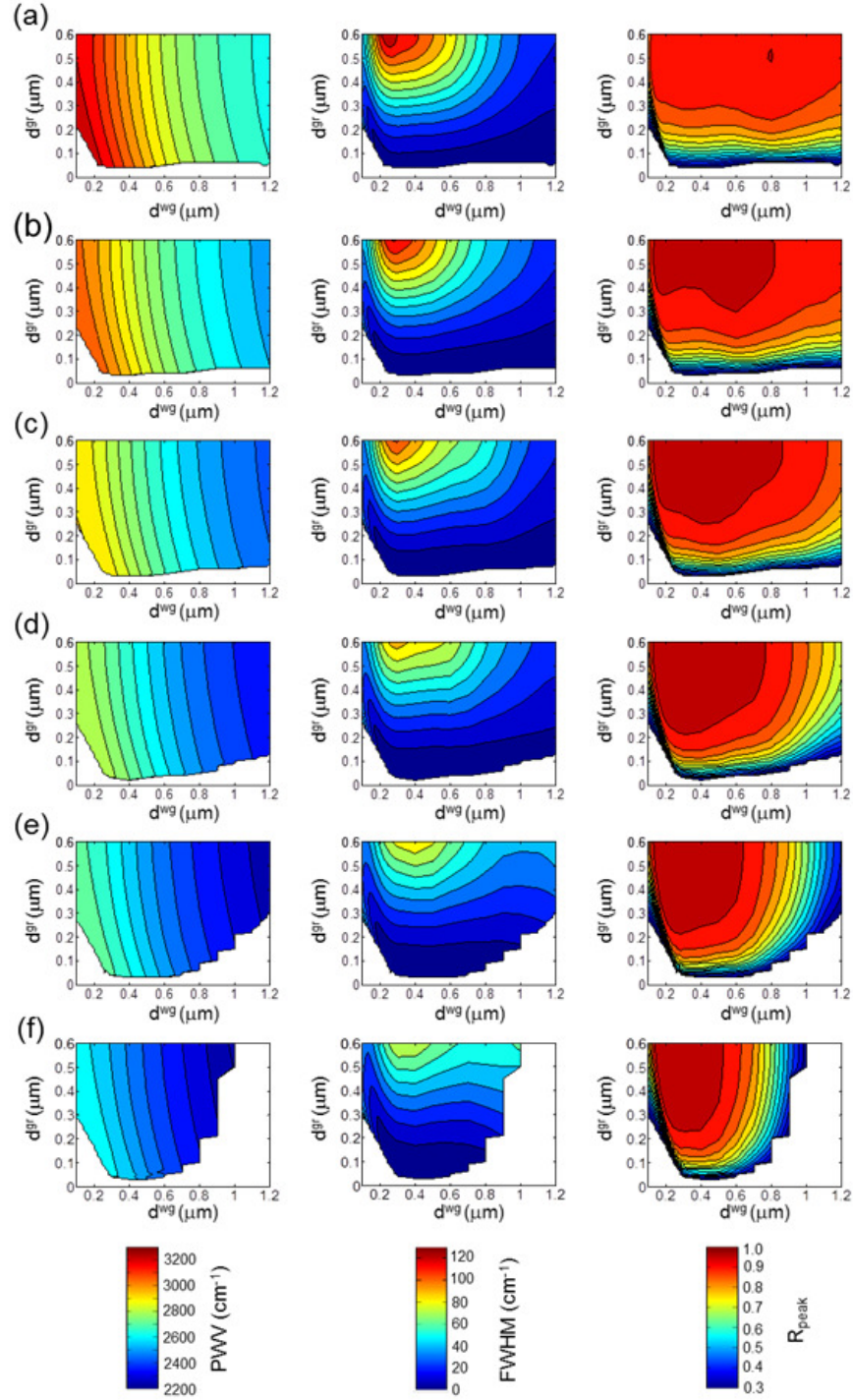


Fig. 6. PWV, FWHM, and R_{peak} of GMR filters with different grating depths (d^{gr}), waveguide layer thicknesses (d^{wg}), and grating periods (Λ): (a) 2.1 μm , (b) 2.2 μm , (c) 2.3 μm , (d) 2.4 μm , (e) 2.5 μm , and (f) 2.6 μm , when a TE-polarized wave is normally incident. The color bar code for PWV, FWHM, and R_{peak} are given below each row.

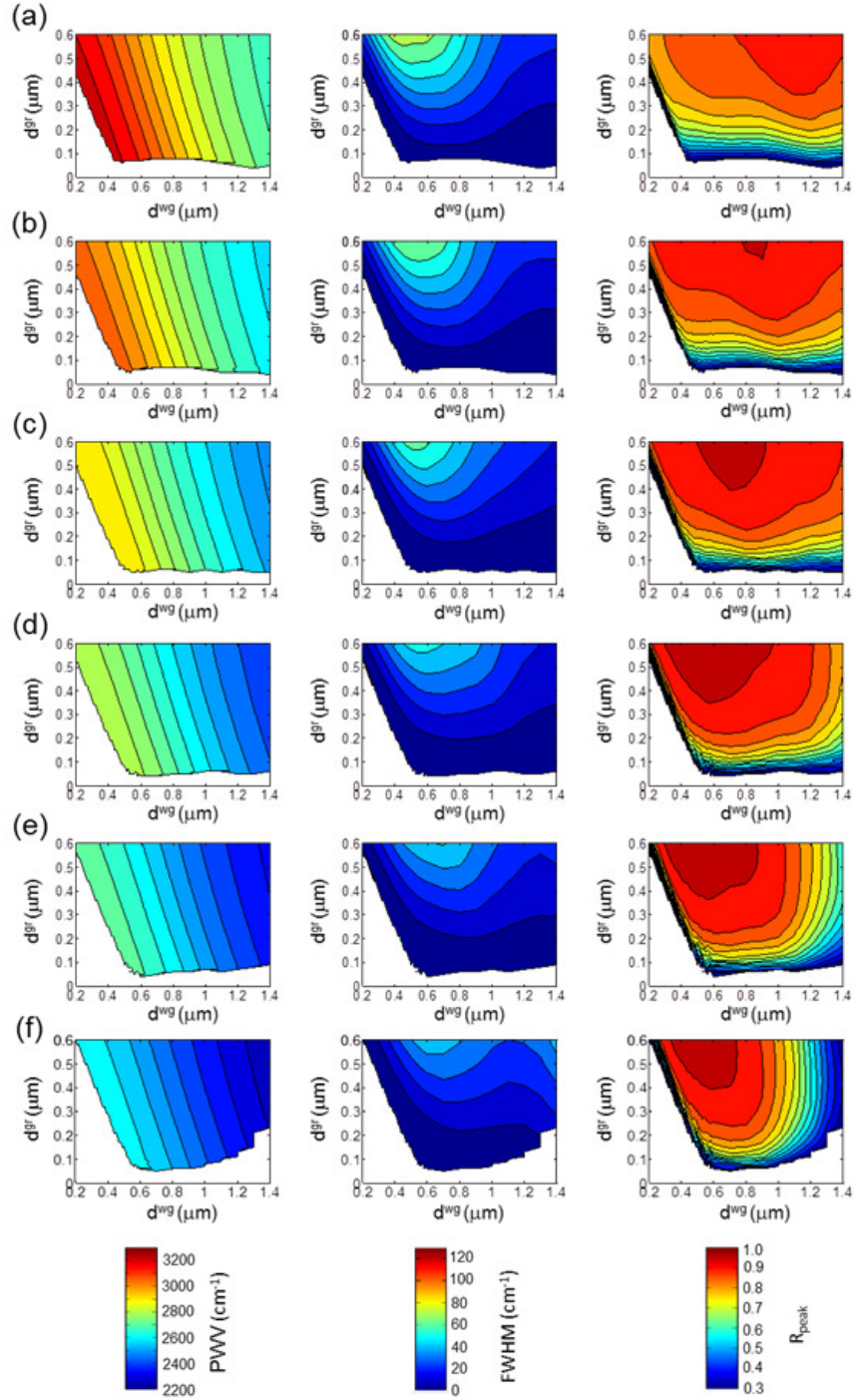


Fig. 7. PWV, FWHM, and R_{peak} of GMR filters with different grating depths (d^{gr}), waveguide layer thicknesses (d^{wg}), and grating periods (Λ): (a) 2.1 μm , (b) 2.2 μm , (c) 2.3 μm , (d) 2.4 μm , (e) 2.5 μm , and (f) 2.6 μm , for TM-polarized normally incident illumination. The color bar code for PWV, FWHM, and R_{peak} are given below each row.

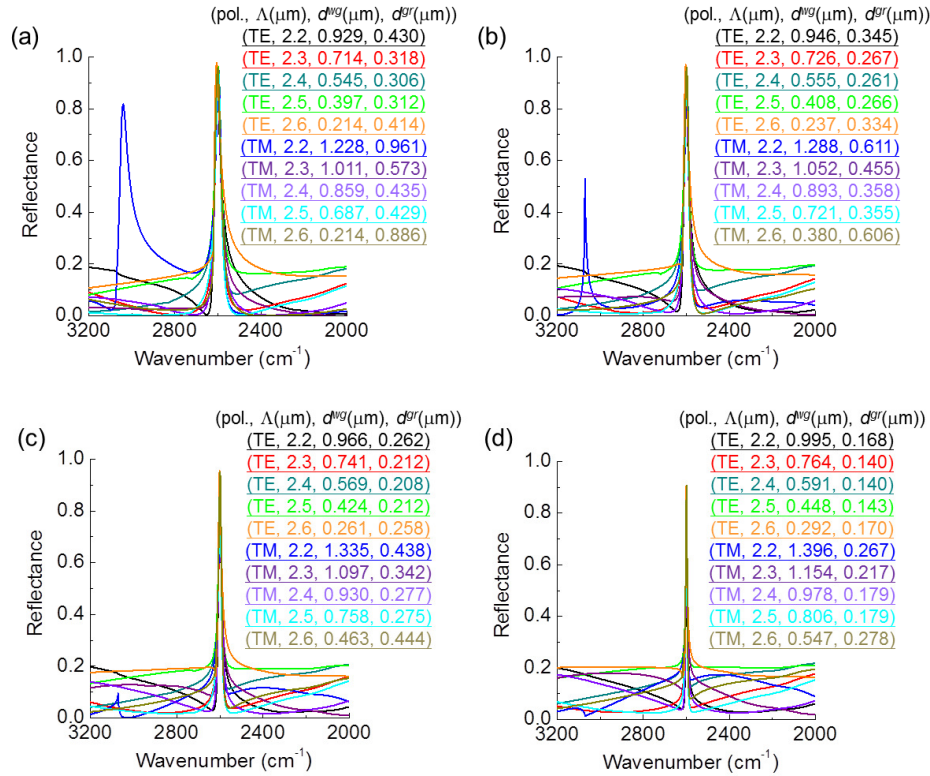


Fig. 8. Design of narrowband GMR filters with PWV of 2600 cm^{-1} for various bandwidths: (a) 32 cm^{-1} , (b) 24 cm^{-1} , (c) 16 cm^{-1} , and (d) 8 cm^{-1} , when a TE or TM-polarized light is normally incident. The grating periods and the layer thicknesses are denoted as a set of numbers.

By combining the contour plots of PWV with the contour plots of bandwidth, we can determine the layer design of GMR filters with a targeted $\text{PWV} = 2600\text{ cm}^{-1}$ for 8, 16, 24, and 32 cm^{-1} bandwidths. Based on Fig. 6 and Fig. 7, when $\Lambda = 1.9\text{--}2.1\text{ }\mu\text{m}$, there is no layer design which can have a $\text{PWV} = 2600\text{ cm}^{-1}$ and $\text{FWHM} \leq 32\text{ cm}^{-1}$. Hence the layer designs of narrowband GMR filters come from contour plots for $\Lambda = 2.2\text{--}2.6\text{ }\mu\text{m}$, and their spectral responses are shown in Fig. 8. To compare performance of the layer designs for a specific PWV and FWHM, we can evaluate their R_{peak} and $I_{\text{IB}}/I_{\text{OB}}$ ratio. Because the $I_{\text{IB}}/I_{\text{OB}}$ ratio depends on the FWHM of the reflection peaks: the larger FWHM, the larger the $I_{\text{IB}}/I_{\text{OB}}$ ratio, the quantity $(I_{\text{IB}}/I_{\text{OB}}) / \text{FWHM}$ measures the band integration ratio per unit bandwidth. Further, we can include R_{peak} , FWHM, and $I_{\text{IB}}/I_{\text{OB}}$ ratio together by defining the figure of merit (FOM) for narrowband GMR filters: $\text{FOM} = R_{\text{peak}} (I_{\text{IB}}/I_{\text{OB}}) / \text{FWHM}$. Here the interval of band integration covers a $2300\text{--}3200\text{ cm}^{-1}$ spectral region because custom IR bandpass filters with the pass band covering the wavenumber range are commercially available. The list of properties for layer designs and their FOM are summarized in the Table. 1, and we can choose the optimal layer design for each bandwidth and polarization by comparing FOMs in each subgroup. A few features may be noticed here. In structures with $\Lambda = 2.2\text{ }\mu\text{m}$ for TM polarization, with layer design denoted in short as a set of polarization and the number of geometric parameters – $\{(\text{TM}, 2.2, 1.228, 0.961), \{(\text{TM}, 2.2, 1.288, 0.611), \{(\text{TM}, 2.2, 1.335, 0.438), \{(\text{TM}, 2.2, 1.396, 0.267)\}$, sideband resonances appear near 3100 cm^{-1} . As the bandwidth of the main peak at 2600 cm^{-1} narrows down from 32 to 8 cm^{-1} , the sideband peak reflectance becomes smaller. Table. 1 shows that the $I_{\text{IB}}/I_{\text{OB}}$ ratio is the determining factor for ranking of the FOM, but R_{peak} of filter designs for the same bandwidth

are very close. The optimal filter designs for different bandwidths have the same grating period $\Lambda = 2.3 \mu\text{m}$ for TE and $\Lambda = 2.5 \mu\text{m}$ for TM. By looking at Fig. 8 the background reflections of the optimal layer designs with $\Lambda = 2.3 \mu\text{m}$ for TE and $\Lambda = 2.5 \mu\text{m}$ for TM do not change appreciably in the region $2300\text{--}3200 \text{ cm}^{-1}$ when the design bandwidth becomes narrower, helping maintain their advantage of high I_{IB}/I_{OB} ratio. In addition, the optimal layer designs for TM polarization has a higher FOM than TE cases because of larger I_{IB}/I_{OB} ratio for TM as shown in Fig. 8 and Table. 1.

Table 1. Summary of Designed GMR Reflectance Filters with a PWV of 2600 cm^{-1} for Various Bandwidths

Targeted bandwidth	(pol., Λ (μm), d^{wg} (μm), d^{gr} (μm))	PWV (cm^{-1})	FWHM (cm^{-1})	R_{peak} (%)	I_{IB}/I_{OB}^a	FOM ^b ($\times 10^{-3} \text{ cm}^{-1}$)
32 cm^{-1}	(TE, 2.2, 0.929, 0.430)	2599.7	31.8	93.2	0.4661	13.6680
	(TE, 2.3, 0.714, 0.318)	2599.9	31.9	93.7	2.2307	65.5776
	(TE, 2.4, 0.545, 0.306)	2599.4	31.9	95.2	0.7709	23.0150
	(TE, 2.5, 0.397, 0.312)	2599.6	31.8	96.5	0.3394	10.2947
	(TE, 2.6, 0.214, 0.414)	2600.2	31.8	97.8	0.2733	8.3997
	(TM, 2.2, 1.228, 0.961)	2600.1	31.8	91.0	0.3234	9.2499
	(TM, 2.3, 1.011, 0.573)	2599.8	31.8	94.1	1.6292	48.1299
	(TM, 2.4, 0.859, 0.435)	2600.1	31.8	94.3	2.3625	70.0357
	(TM, 2.5, 0.687, 0.429)	2600.1	31.8	95.2	17.7538	530.6849
	(TM, 2.6, 0.214, 0.886)	2599.9	31.8	95.7	3.2365	97.4794
	(TE, 2.2, 0.946, 0.345)	2599.5	23.8	91.5	0.3561	13.6672
	(TE, 2.3, 0.726, 0.267)	2599.9	23.8	91.8	1.2487	48.2469
	(TE, 2.4, 0.555, 0.261)	2599.7	23.9	94.0	0.4152	16.3342
	(TE, 2.5, 0.408, 0.266)	2600.1	23.8	95.6	0.2120	8.5028
	(TE, 2.6, 0.237, 0.334)	2599.7	23.8	97.1	0.1830	7.4620
24 cm^{-1}	(TM, 2.2, 1.288, 0.611)	2600.0	23.8	91.5	0.7202	27.6792
	(TM, 2.3, 1.052, 0.455)	2600.1	23.8	93.0	0.5400	21.0906
	(TM, 2.4, 0.893, 0.358)	2599.9	23.8	93.0	0.9343	36.5372
	(TM, 2.5, 0.721, 0.355)	2600.2	23.9	94.1	2.7034	106.5626
	(TM, 2.6, 0.380, 0.606)	2599.8	23.8	95.9	1.2659	51.0744
	(TE, 2.2, 0.966, 0.262)	2599.7	15.8	87.6	0.2255	12.4884
	(TE, 2.3, 0.741, 0.212)	2599.8	15.9	88.5	0.5935	33.0757
	(TE, 2.4, 0.569, 0.208)	2599.9	15.8	91.2	0.2029	11.6988
	(TE, 2.5, 0.424, 0.212)	2600.1	15.8	93.6	0.1181	7.0085
	(TE, 2.6, 0.261, 0.258)	2599.5	15.9	95.5	0.1114	6.7021
	(TM, 2.2, 1.335, 0.438)	2599.9	15.8	89.5	0.3127	17.7129
	(TM, 2.3, 1.097, 0.342)	2600.1	15.8	90.3	0.2055	11.7573
	(TM, 2.4, 0.930, 0.277)	2600.1	15.8	90.3	0.3884	22.1582
	(TM, 2.5, 0.758, 0.275)	2600.6	15.8	91.7	0.8751	50.7937
	(TM, 2.6, 0.463, 0.444)	2600.1	15.8	95.0	0.3801	22.7944
8 cm^{-1}	(TE, 2.2, 0.995, 0.168)	2599.7	7.8	76.1	0.0926	9.0359
	(TE, 2.3, 0.764, 0.140)	2599.9	7.8	77.7	0.1858	18.5013
	(TE, 2.4, 0.591, 0.140)	2599.9	7.8	83.8	0.0719	7.7254
	(TE, 2.5, 0.448, 0.143)	2599.9	7.8	87.5	0.0474	5.3026
	(TE, 2.6, 0.292, 0.170)	2599.8	7.8	90.5	0.0486	5.6220
	(TM, 2.2, 1.396, 0.267)	2600.0	7.9	81.5	0.0785	8.1481
	(TM, 2.3, 1.154, 0.217)	2599.7	7.9	82.0	0.0627	6.5519
	(TM, 2.4, 0.978, 0.179)	2599.9	7.8	81.1	0.1206	12.5280
	(TM, 2.5, 0.806, 0.179)	2600.2	7.8	84.4	0.2531	27.5174
	(TM, 2.6, 0.547, 0.278)	2600.1	7.8	90.7	0.1056	12.2939

^aThe ratio of I_{IB} to I_{OB} is used to evaluate the influence of sideband or background reflections.

^bFigure of merit (FOM) for narrowband GMR reflectance filters is $\text{FOM} = R_{\text{peak}} (I_{IB}/I_{OB}) / \text{FWHM}$.

By using a design optimization process that considers the magnitude of reflected intensity at wavelengths other than the resonant wavelength, it becomes possible to design narrowband GMR filters that can efficiently reflect a narrow band of wavelengths appropriate for use in spectrometers, even in the presence of optical losses in the device materials. The forgoing analysis assumes that the incident illumination is perfectly collimated. Light emitted by

extended thermal sources used in spectrometers, however, is not perfectly collimated. Because the spectral response of narrowband GMR filters is very sensitive to the incident angle [23], such angle of divergence arising from imperfect collimation can degrade the performance of narrowband GMR filters by reducing peak reflectance and broadening filter bandwidth [36]. The trade-off between narrow bandwidth and performance limitation by imperfect collimation must also be taken into consideration when selecting bandwidth of GMR filters for DFIR spectroscopy, and this will be a topic of a future publication.

The I_B/I_{OB} ratio depends on the spectral interval of integration. If the spectral interval of integration becomes wider than the region of 2300-3200 cm^{-1} , the sideband reflections will increase for optimal layer designs but decrease for others, making the advantage of optimal layer designs for having low background reflections near the resonance wavenumber of 2600 cm^{-1} indistinguishable. By co-locating optimized narrowband GMR filters with one IR bandpass transmission filter with wide bandwidth such as 2300-3200 cm^{-1} , the optical power outside the pass band can be blocked, and the signal from the small spectral region of interest can then be further improved with high I_B/I_{OB} ratio powered by the optimal layer design.

3.4 Comparison to the antireflection thin-film equivalence method

It is meaningful to compare the optimal layer design of GMR filters developed in this paper with the conventional design method with antireflection (AR) thin-film equivalence concept [26, 37]. For double-layer GMR filter structures, AR conditions for TE require that layer thicknesses of grating layer and waveguide layer are $m\lambda_{\text{res}}/4(\epsilon_{\text{gr,eff}})^{1/2}$ and $m\lambda_{\text{res}}/4(\epsilon_{\text{wg}})^{1/2}$, respectively, where $m = 1, 3, 5, \dots$, $\epsilon_{\text{gr,eff}} = (\epsilon_c + \epsilon_{\text{SiN}})/2$, $\lambda_{\text{res}} = 1/\text{PWV}$, and $\epsilon_c = 1$ (air). Here we choose $m = 1$ because smaller grating depth can result in narrower bandwidth, which is favorable for applications to IR spectroscopy. Because the imaginary part of the permittivity of Si_3N_4 at 2600 cm^{-1} is $\sim 2.2 \times 10^{-3}$, which is much smaller than the real part of its permittivity (~ 4.04), we use the real part of permittivity in Si_3N_4 approximately in the AR design. In Fig. 9(a) the blue curve shows the spectral response of the filter with AR design, where $d^{\text{gr}} = 0.606 \mu\text{m}$ and $d^{\text{wg}} = 0.478 \mu\text{m}$. The grating period $\Lambda = 2.42 \mu\text{m}$ is finely adjusted to match the filter resonance wavenumber with the targeted 2600 cm^{-1} , as shown in the inset.

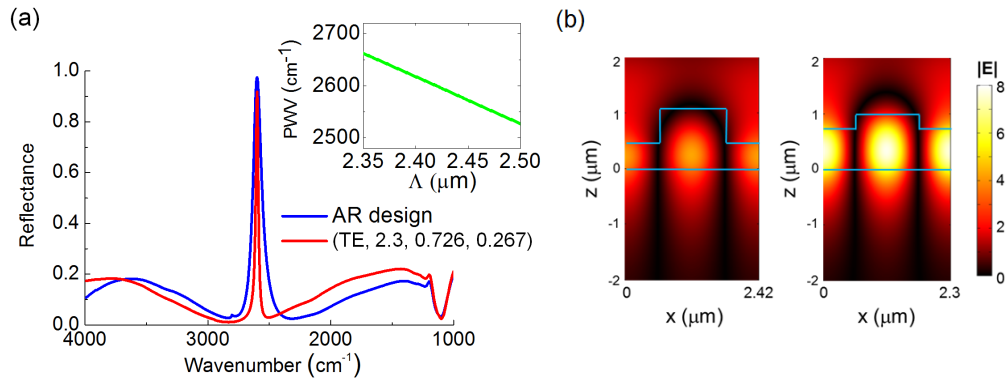


Fig. 9. (a) Comparison of GMR filter designs for TE PWV of 2600 cm^{-1} using AR thin-film equivalence concept (blue) and using our optimal design method for 24 cm^{-1} bandwidth and the same fitted PWV (red), when TE-polarized light is normally incident. The FWHM bandwidth of the AR designed filter is 86 cm^{-1} . Inset: PWV vs. the grating period for GMR filters with AR thin-film equivalent thicknesses at the specified wavenumber of 2600 cm^{-1} . The layer thicknesses are $d^{\text{wg}} = 0.478 \mu\text{m}$ (quarter-wave) and $d^{\text{gr}} = 0.606 \mu\text{m}$ (quarter-wave). The grating period is tuned to match the targeted PWV of 2600 cm^{-1} , resulting in the grating period $\Lambda = 2.42 \mu\text{m}$ for the AR designed filter. (b) E-field enhancement distribution for TE polarization in the GMR structure using AR approximation design at a resonance wavenumber of 2600 cm^{-1} (left) and in the structure using optimal design method for 24 cm^{-1} bandwidth at a resonance wavenumber of 2599 cm^{-1} (right).

In Fig. 9(a) the red curve shows the optimal layer design {TE, 2.3, 0.726, 0.267} for bandwidth of 24 cm^{-1} . However, the FWHM bandwidth of the filter with AR equivalence design is 86 cm^{-1} , which is not narrow enough to detect the signal in the narrow spectral region of interest in routine IR spectroscopy. The large bandwidth of the filter with AR design arises because the modulation index, $(\epsilon_{\text{SiN}} - \epsilon_{\text{Air}})/(\epsilon_{\text{SiN}} + \epsilon_{\text{Air}}) = 0.60$, is too large to correctly model the heavily modulated grating layer with effective permittivity [37]. Incorporating one more layer in the surface-relief filter structures (triple-layer GMR filters) may further reduce sidebands of the filters with AR design, but the resonance linewidth cannot be effectively improved because the bandwidth of GMR filters is mainly determined by the magnitude of the modulation index. The minimum out-of-bandpass reflections of the filter with AR design and the filter created with the optimal design method are 2.5% and 1.2% near resonance, respectively, indicating that the optimally designed filter can have narrower linewidth without sacrificing low out-of-bandpass reflections. In Fig. 9(b) the on-resonance E-field enhancement distributions of the two filters are compared, which shows that the filter with optimal design {TE, 2.3, 0.726, 0.267} has a higher maximum field enhancement due to narrower linewidth and longer photon lifetime. Besides the optimized filters for 24 cm^{-1} bandwidth, filters with optimal layer designs for narrower bandwidths such as 8 and 16 cm^{-1} can have narrower linewidth and greater E-field enhancement factor at a specific resonance wavenumber, which are promising for applications to optical sensing in mid-IR as well as DFIR spectroscopy.

Although GMR filters are polarization dependent, DFIR spectroscopy requires only one polarization. Therefore, optimally designed narrowband GMR filters presented in this work can serve this specific purpose. However it is also interesting to consider polarization independent optical filters such as two-dimensional periodic grating filters or photonic crystals [38].

4. Conclusions

In summary, we demonstrate design optimization of narrowband GMR filters in the mid-IR, with absorption and dispersion properties of materials taken into consideration. We illustrate the effect of absorption on GMR filters with narrow bandwidth, which limits the performance of GMR filters by creating a trade-off between filter bandwidth and peak reflectance. The optimal design method developed in this work provides high-performance GMR filter designs with accurate control of filter resonance wavenumber, reduced background reflection, and various narrow bandwidths. Based on the same index modulation value, the designed filter by the AR equivalence method has a bandwidth of 86 cm^{-1} , but the designed filters with the optimal design method developed here can have bandwidth smaller than 32 cm^{-1} without sacrificing low sideband reflections near resonance. We anticipate that the optimal design method developed here will guide the design and fabrication of narrowband GMR filters for DFIR spectroscopy and many other applications that can take advantage of the unique properties of GMR filters.

Acknowledgments

This work was funded by the National Institutes of Health (grant number R01 EB009745A). J. N. Liu acknowledges the support of Taiwan's Government Fellowship for Studying Abroad.